

Addendum  
Electronics Division Internal Report  
No. 312

October 20, 2004

**Abstract**

NRAO Electronics Division Internal Report 312, published September 2, 2003, described investigations into the character and causes of the Green Bank Telescope spectral baselines. Since publication, several steps have been taken to further understand and mitigate some of the causes of unsatisfactory baselines. This Addendum to EDIR 312 will review the steps taken and additional knowledge obtained to date, and describe future plans.

# 1 Review

Spectroscopy in radio astronomy is generally done by measuring the system output spectra under two conditions: one ( $S_r$ ) with the beam on a reference position, and a second ( $S_s$ ) on the source of interest. On the GBT, the switching is accomplished by position switching (moving the antenna position), and/or by beam switching (available at frequencies above 12GHz). To understand the analysis of position switched data, it is useful to model the receiver chain with a power gain transfer function  $G(f)$  and noise temperature  $T_{rx}(f)$ . As indicated, both of these quantities are functions of frequency and summarize the cascade of many active and passive components. Our system consists of the antenna, the receiver chain, and a spectrometer used to measure the output power spectrum. The equation for the system output power spectrum may be written as:

$$S_o(f) = (T_{sor}(f) + T_{ant}(f) + T_{rx}(f))k_B G(f) \quad (1)$$

where  $T_{sor}$  represents the effective temperature of the antenna main beam,  $T_{ant}$  the amalgamation of noise due to atmosphere, background, spillover, etc.,  $T_{rx}$  is the noise temperature of the receiver and feed, and  $k_B$  is the product of Boltzmann's constant and the effective bandwidth of each spectrometer frequency channel. (Note that each noise component is or may be a function of frequency, but from this point on we will omit the  $(f)$  except when it seems important to emphasize the frequency variation.) We can now write equations for output spectra  $S_s$  and  $S_r$ . The receiver gain and noise temperature are in general functions of time, if not signal level, so we will also distinguish the gain and noise values during the respective spectral measurements with  $s$  and  $r$  subscripts.

$$S_r = (T_{ref} + T_{ant,r} + T_{rx,r})k_B G_r \quad (2)$$

$$S_s = (T_{sig} + T_{ant,s} + T_{rx,s})k_B G_s \quad (3)$$

Because the system gain function has relatively large variations with frequency, we calculate the ratio of the two scans which under certain conditions will cancel the gain function:

$$\frac{S_s}{S_r} - 1 = \frac{S_s - S_r}{S_r} = \frac{(T_{sig} + T_{ant,s} + T_{rx,s})G_s - (T_{ref} + T_{ant,r} + T_{rx,r})G_r}{(T_{ref} + T_{ant,r} + T_{rx,r})G_r} \quad (4)$$

regrouping we obtain,

$$\frac{S_s - S_r}{S_r} = \frac{(T_{sig}G_s - T_{ref}G_r) + (T_{ant,s}G_s - T_{ant,r}G_r) + (T_{rx,s}G_s - T_{rx,r}G_r)}{(T_{ref} + T_{ant,r} + T_{rx,r})G_r} \quad (5)$$

The quantity of interest is  $T_{sig}(f) - T_{ref}(f)$ , and to pluck this value from equation 5, it is first necessary that the system gain and noise temperature are

completely stable over the measurement period. That is  $G_s = G_r$ ,  $T_{ant,s} = T_{ant,r}$ , and  $T_{rx,s} = T_{rx,r}$ . Then equation 5 becomes:

$$\frac{S_s - S_r}{S_r} = \frac{T_{sig} - T_{ref}}{T_{ref} + T_{ant,r} + T_{rx,r}} \quad (6)$$

This equation shows that, even with perfect system stability during the measurement, the quantity  $(S_s - S_r)/S_r$  will only be flat with frequency if  $T_{ref} + T_{ant,r} + T_{rx,r}$  is flat, or  $T_{sig} - T_{ref}$  is very small over most of the frequency range. The denominator of equation 6 is just  $T_{sys}(f)$  during the reference scan, so multiplying by that value will retrieve the desired quantity  $T_{sig} - T_{ref}$ .  $T_{sys,r}$  is usually determined by using a small injected noise cal, but for flat baselines  $T_{sys,r}$ , and hence  $T_{cal}$ , must be determined to a high accuracy at every frequency in the passband. The importance of this increases as the average difference between  $T_{sig}$  and  $T_{ref}$  gets larger (spectroscopy on continuum sources). In the past, spectral data analysis has generally assumed a constant  $T_{cal}$  and/or  $T_{sys}$  across the spectrum, or at most a fit to a few points, but with the broad bandwidths available from the GBT spectrometer, in many cases that turns out to be an unsatisfactory approach.

It is clear from this discussion that gain or noise temperature changes during a measurement will prevent the cancellation of quantities in equation 5. And, ripple in  $T_{sys}$  must be minimized or measured accurately in order to cancel the denominator of equation 6.

The past year's work on GBT baselines has focused on three broad areas:

**Gain Stability** The degree of stability required is challenging. Most of the identified problems were related to coaxial interconnections, and were addressed by improved testing and assembly procedures.

**Standing Waves** As discussed in the body of EDIR 312, standing waves impact the system by producing frequency structure in both gain and noise temperature. The standing wave stability is affected by changes in mismatch magnitude or phase, and by changes in the electrical length of transmission paths. The effects can be attacked by reducing the magnitude of mismatches, stabilizing the electrical length of transmission lines, or shortening transmission lines (which increases the period of the ripple and may make it easier to tolerate).

**Receiver Noise Ripple** Extensive testing has shown that frequency structure in receiver noise temperature is a major source of difficulties in observing strong continuum sources. Little progress beyond what was described in the body of EDIR 312 has been made in reducing the structure, but some progress has been made in the understanding and in calibration methods.

Discussion of specific areas of work follow.

## 2 Coaxial Cables

PTFE (Teflon), the most common dielectric found in microwave cables, has an unfortunate transition in its physical properties near room temperature. That leads to high sensitivity of electrical length to temperature (about 100ppm/ $^{\circ}C$ ). As described in EDIR 312, section 4.4, a couple of varieties of Andrews Helix type cables using polyethylene dielectric have significantly better temperature coefficients, and have been installed in several critical locations. Occasional problems with the FSJ1-50A Helix developed due to shearing of the copper jacket at the SMA connector clamp-on backshell. These failures caused gain instabilities that were intermittent and position dependent. An assembly procedure was developed that supplemented the clamp with epoxy potting, and has largely eliminated cable failures due to this cause. Connector problems with other Helix cable types have occurred, and one must be careful in their use, despite the attractive performance of the cable itself.

Longer PTFE cables in the Equipment Room between the Converter Racks and the Spectrometer were placed in conduits to buffer air temperature fluctuations. These cables carry lower frequencies and the cost of retrofitting to Helix does not yet seem necessary. Ripple components consistent with the cable lengths have not been observed in baselines since the buffering was installed.

## 3 Feed Radomes

The Gregorian feeds have woven PTFE sheets over the feed apertures, and water on this surface leads to reflections that are unstable as the water moves around. The radome blower system was upgraded to increase the air flow, significantly improving the removal of water beads.

The original radome designs used flat metal rings to clamp the PTFE sheets to the feed horns. That led to a recess in which water tended to puddle. All the feeds at X-band and above have now been retrofitted to use a wrap-around design for radome attachment, eliminating the recess.

## 4 Converter Rack

EDIR 312 section 4.5 described a persistent baseline ripple component with period near 60MHz, whose origin had been isolated to the Converter Racks and was closely related to the Equipment Room temperature. The magnitude of this ripple ranged up to about 0.5% of the total power. The generating mechanism was not well understood however, and effort was spent both to improve the temperature stability, and to understand how the ripple was generated.

Figure 1 shows a simplified view of the interface between the IF Optical Receiver and the 1-8 GHz Converter modules. The IF signal is amplified and split four ways in the Optical Receiver, and then goes to four Converter modules (only two of the four Converter modules are shown in the figure). The baseline ripple generating mechanism is understood by tracing a signal through the

diagram: A signal leaves the amplifier and is split four ways in the power divider, which has electrical delay  $\Theta_d$ . The one-fourth signal that exits the lower port travels through a fairly long coaxial cable with delay  $\Theta_2$  and enters the Converter module input switch and mixer. However, a portion of the signal is reflected by reflection coefficient  $\rho_2$ , back thru the cable delay  $\Theta_2$  and the power divider and into the amplifier output port. At the amplifier output, a portion is reflected,  $\rho_a$ , and reenters the splitter input. So, the total signal that enters the top converter module mixer is the vector sum of one-fourth of the amplifier output signal, and a smaller component which has travelled through  $\Theta_d$  and  $\Theta_2$  twice. (And two other components off the other two converter modules not shown.) These reflected signals cause standing waves and hence gain ripples with frequency. Note that if the phase of the reflected signals change due to, say, change in the electrical phase of the cable delay  $\Theta_2$ , or reflection coefficients  $\rho_2$  or  $\rho_a$ , the gain ripple will change resulting in baseline ripples. Early on, the mechanism of change in the cable delay was recognized and phase stable cables were installed. However, the ripples were still apparent and the search began for other causitive mechanisms. In the end, the problems were found to be dominated by a few highly sensitive, defective components - RF switches, pads, etc. Because a defective component affects the response of four channels and the effects tend to be too small to detect with common test equipment, isolating the problems proved to be difficult.

Figure 2 shows a series of two-minute off/on baselines taken through the system illustrating the improvements that have been achieved. Although significant improvements have been made, some ripple is still apparent. This ripple does tend to average out over many off/on pairs. The final solution however probably lies in repackaging of this area of the system to greatly shorten the pathlengths involved and to provide improved thermal buffering.

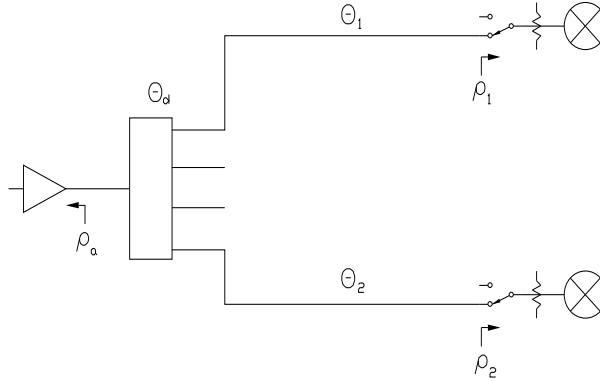


Figure 1: A simplified block diagram of the Optical Receiver - Converter Module interface.

## 5 Receiver Noise

### 5.1 Introduction

Section 3 of EDIR 312 discussed spectral baselines on continuum sources. It was recognized that receiver noise which varies with frequency is a potential source of baseline problems because usual data analysis techniques assumed a constant  $T_{sys}(f)$ . The search for causes of ripple in receiver noise focused on the receiver input area - between the feed aperture and the first LNA - and in fact a few specific problems were identified and corrected as discussed in the original report. However, it became clear that this was not the whole story - the shape of the baselines were too irregular and the period of ripples did not match physical lengths that could set up standing waves. One difficulty in understanding the problem was because our normal laboratory equipment and methods of measuring noise temperature provided frequency resolution too coarse to be of much use. However, the GBT spectrometer obviously provides a means to obtain high-resolution spectra, and as long as the total power does not change by more than 3dB or so, we felt it could be used to perform a hot-cold noise temperature measurement. We put together an experiment using components taken from the GBT 40-52 GHz Q-band receiver, with care taken to eliminate the possibility of input mismatch or resonances affecting the results.

A test arrangement consisting of a cooled LNA and mixer, IF filter, and IF amplifier were taken from the Q-band receiver and placed in one of our test dewars. The LNA input port was connected to a cooled rectangular waveguide load. The load was thermally separated from the LNA with a 1 cm stainless steel waveguide shim. A small heater and temperature sensor allowed the load

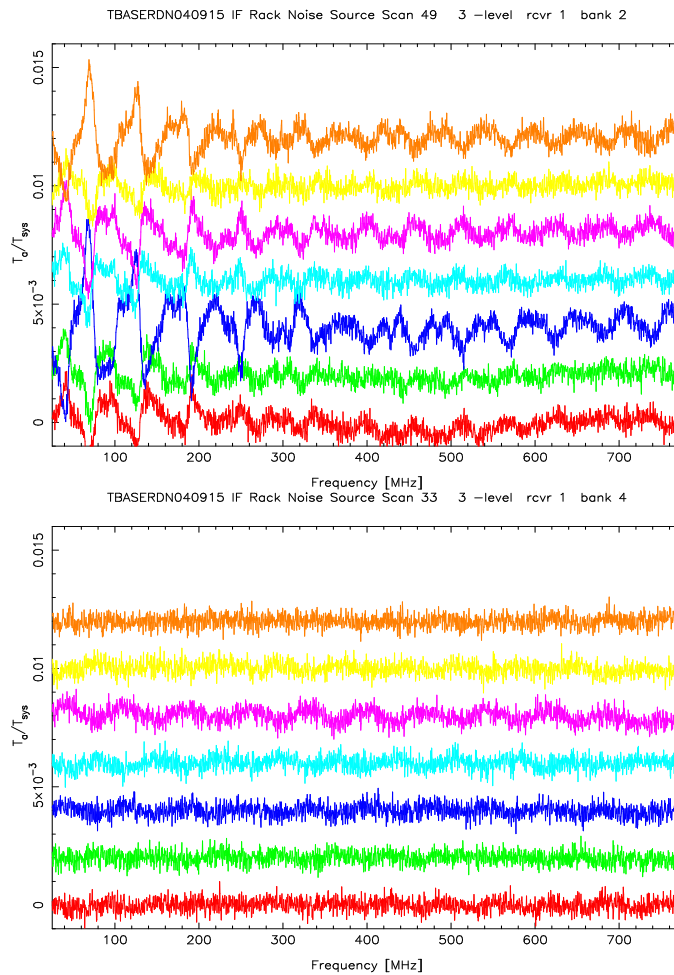


Figure 2: IF system baseline ripples due to Equipment Room temperature before (top panel) and after (bottom panel) improvements to the Converter Rack equipment.

temperature to be adjusted by 10-15K. Measurements on the stainless shim and the load show that the combination has a return loss of 32 dB or better.

The test dewar was located in the Equipment Room and the IF output (centered at 6 GHz) was connected into the GBT IF system via heliax cable. The system and the spectrometer were then configured for 800 MHz bandwidth measurements of the spectrum.

## 5.2 The Y-factor Method

The most common engineering method of determining a receiver's noise temperature is to measure its output power with two known input source temperatures. The ratio of the two powers is termed the Y-factor. Since a spectrometer measures the spectral power versus frequency, we can use two measurements taken with two source temperatures to obtain  $Y(f)$ :

$$Y(f) = \frac{S_{hot}}{S_{cold}} = \frac{(T_{hot} + T_{rx,hot}(f))k_B G_s}{(T_{cold} + T_{rx,cold}(f))k_B G_r} \quad (7)$$

Again assuming receiver stability, and solving for  $T_{rx}$ , we obtain a familiar equation:

$$T_{rx}(f) = \frac{T_{hot} - Y(f)T_{cold}}{Y(f) - 1} \quad (8)$$

## 5.3 Q-band Laboratory Data

Spectra were measured with two load temperatures differing by about 15K, and the data used to calculate  $T_{rx}(f)$  using equations 7 and 8. Figure 3 plots typical  $T_{rx}$  using this method. To check linearity and stability of the data, several subsequent scans taken at a variety of load temperatures were processed through the baseline equations using this measured  $T_{rx}$ . Figure 4 shows the effect on spectral baselines when the measured  $T_{rx}$  is used in equation 6.

The fact the input load return loss was quite low makes a strong case that the source match seen by the LNA can not explain the noise structure seen in these measurements. Subsequent work indicates that in this receiver mixer noise is a significant contributor to the total receiver noise structure, and can perhaps be mitigated by increasing the gain before the mixer and by terminating the image and other sideband frequencies with low VSWR. Work along these lines is on-going, and may lead to similar investigations in other receivers.

## 5.4 X-band Astronomical Data

Because of the laboratory results, it seemed possible that the  $T_{rx}$  variations have been a major source of baseline structure when observing continuum sources. And, it might be possible to use astronomical observations to measure  $T_{rx}$  for subsequent use in baseline data analysis.

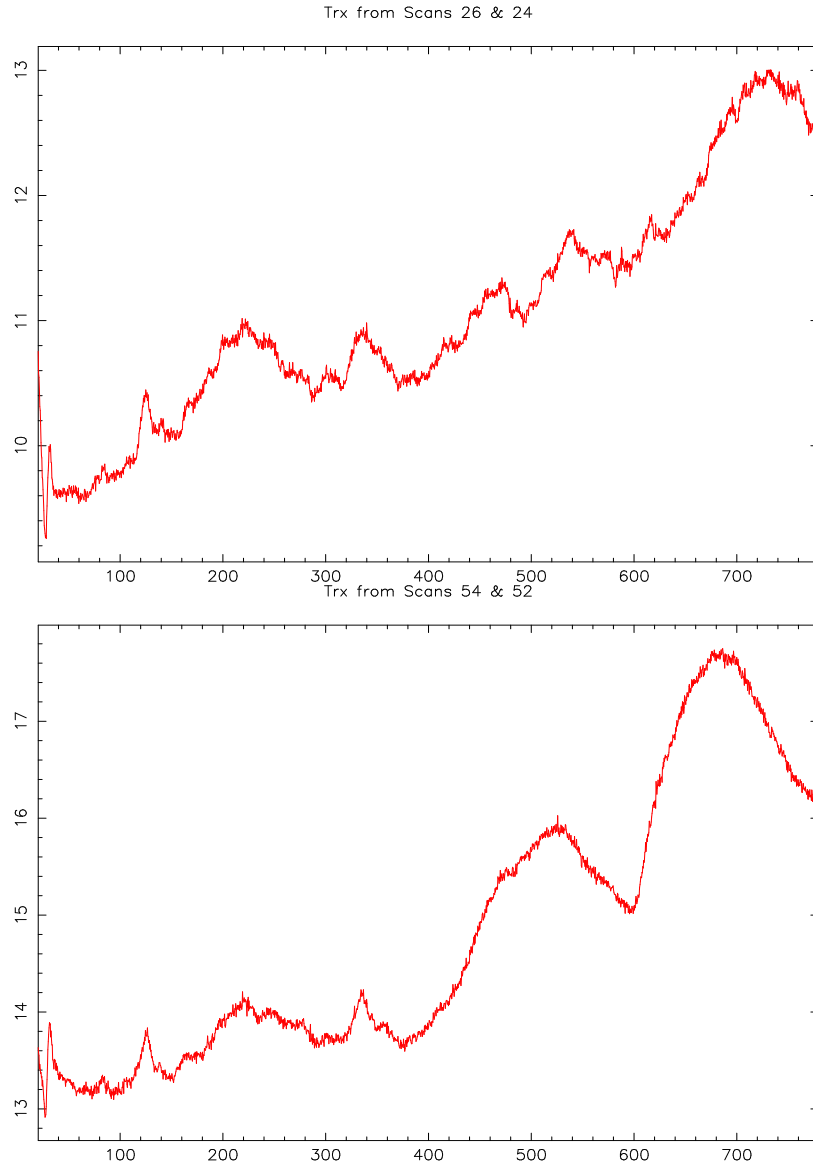


Figure 3:  $T_{rx}$  at 42 GHz (upper panel) and 43 GHz (lower panel), obtained from a test dewar containing a Q-band LNA and cooled mixer, calculated with equations 7 and 8. A heated waveguide termination was used to vary the LNA input load temperature.

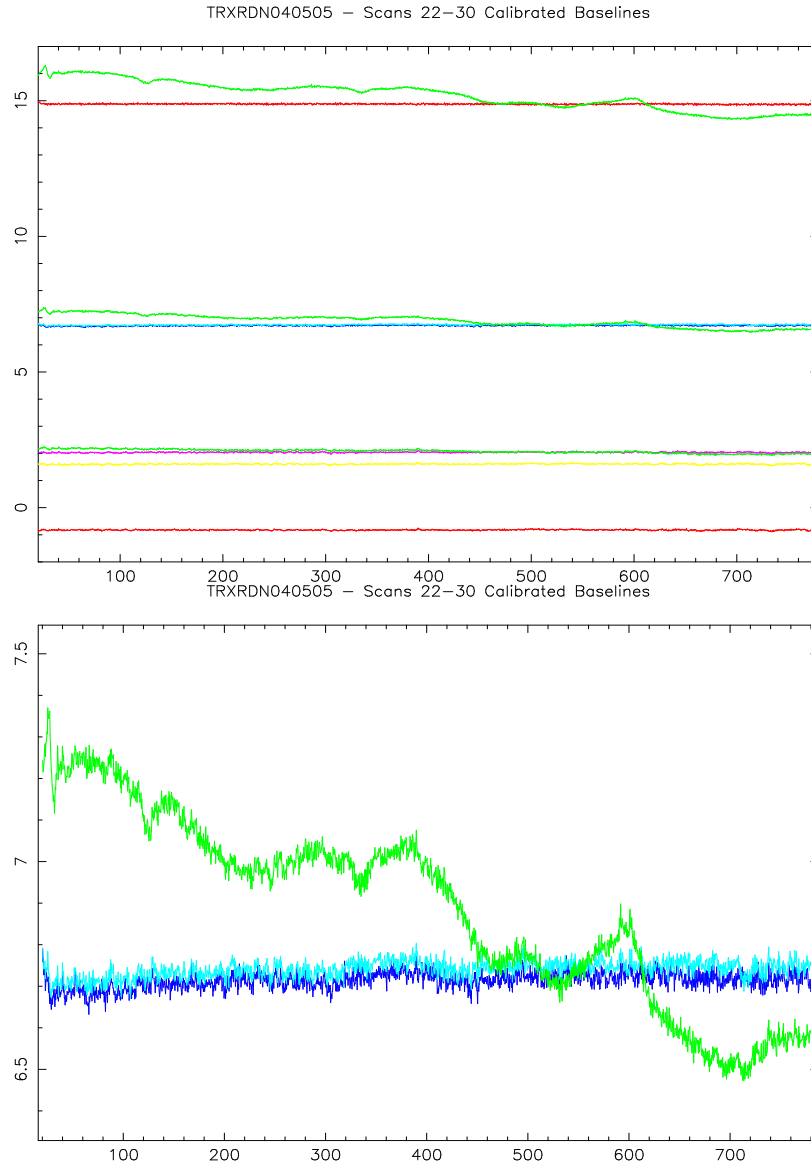


Figure 4: The upper plot shows the spectral baselines on the Q-band test dewar setup for several signal scans taken at various load temperatures. The green traces were calculated using a mean  $T_{rx}$  of 15.5K, and the other (flatter) traces used measured  $T_{rx}(f)$ . The lower panel zooms into the region around 7 K.

To see how the Y-factor measurement of  $T_{rx}(f)$  behaves with a front-end operating on the GBT, astronomical data previously taken with the X-band receiver was analyzed. The first data set consisted of a sequence of on-off observations of NGC 7027. One observation was used to calculate  $T_{rx}$ , and that value used to analyze subsequent observations. Only one source was observed, but the data can provide an indication of the stability of the analysis. Examples from this dataset are shown in Figures 5 and 6.

The second X-band data set analyzed was a sequence of on-off observations of three sources. By coincidence, one of the sources was NGC 7027, and that source was used to determine  $T_{rx}$  applied to analysis of the other sources. The results are shown in Figures 7 and 8.

It is clear from these figures that the technique used here has promise in removing major portions of the baseline structure on continuum sources. However, other uncertainties are introduced by the need to understand well the spectral signature of calibrator sources. Work continues to develop the best and most practical observing and analysis procedures.

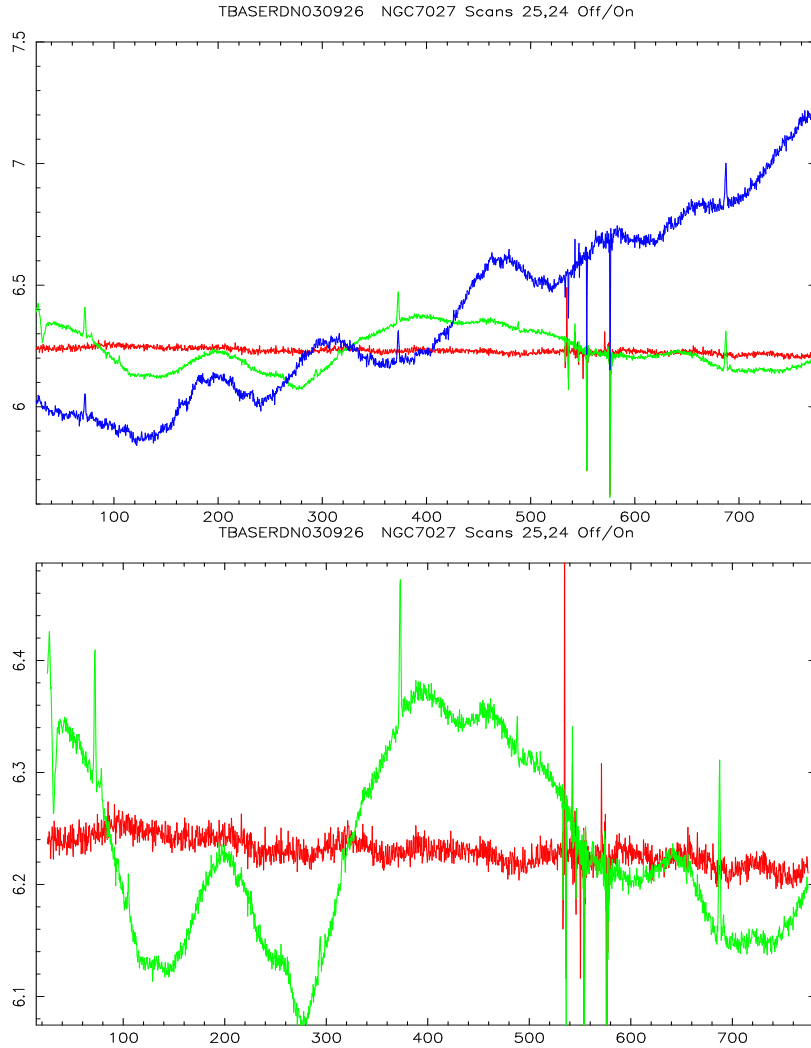


Figure 5: X-band spectral baselines calculated for TBASERDN030926 scan pair 24 and 25, ACS Bank A. The red trace was calculated using  $T_{rx}$  measured using scan pair 22 and 23 data as a Hot/Cold measurement. The green trace was calculated using a constant  $T_{sys}$ , and the blue trace used a  $T_{sys}$  derived from Cal On - Cal Off data in scan 25. The vertical scale corresponds to  $T_{On} - T_{Off}$  in Kelvin. The lower panel shows the red and green traces in more detail. For these plots 400MHz on the horizontal axis corresponds to a sky frequency of 9000MHz, and sky frequency increases to the right. The data was from the RCP polarization.

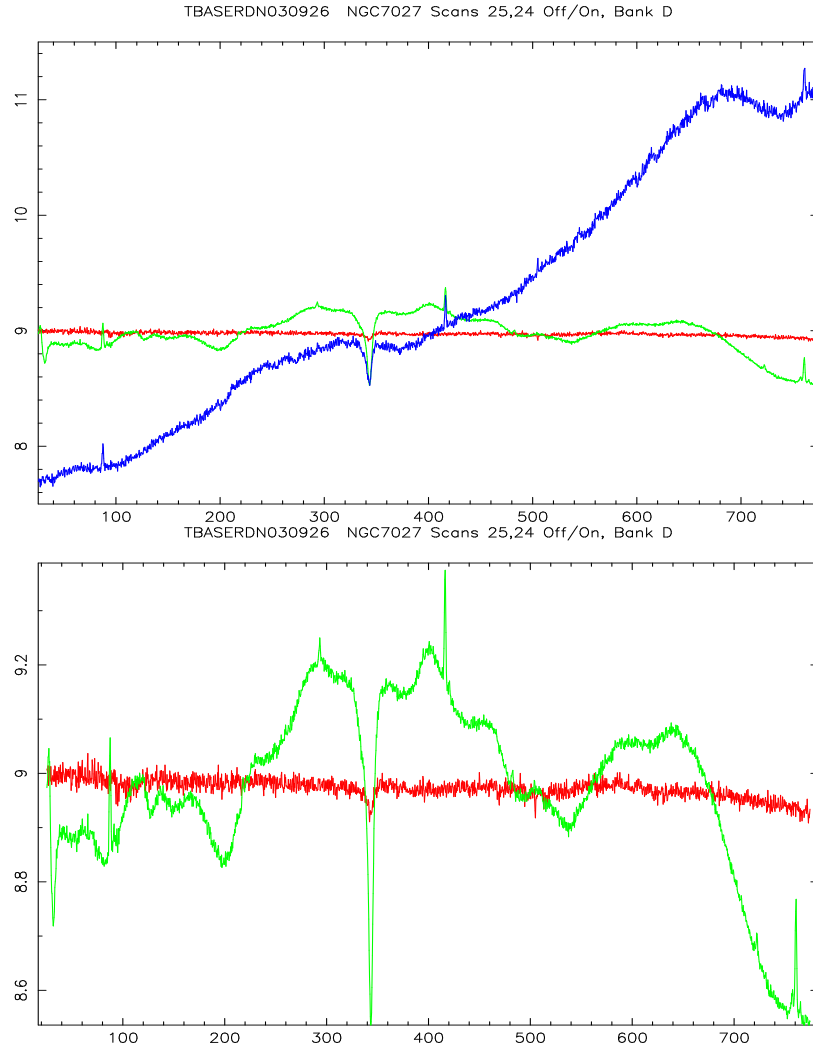


Figure 6: X-band spectral baselines calculated for TBASERDN030926 scan pair 24 and 25, ACS Bank D, calculated in three ways. The red trace was calculated using  $T_{rx}$  measured using scan pair 22 and 23 data as a Hot/Cold measurement. The green trace was calculated using a constant  $T_{sys}$ , and the blue trace used a  $T_{sys}$  derived from Cal On - Cal Off data in scan 25. The vertical scale corresponds to  $T_{On} - T_{Off}$  in Kelvin. The lower panel shows the red and green traces in more detail. For these plots 400MHz on the horizontal axis corresponds to a sky frequency of 9600MHz, and sky frequency increases to the right. The data was from the RCP polarization.

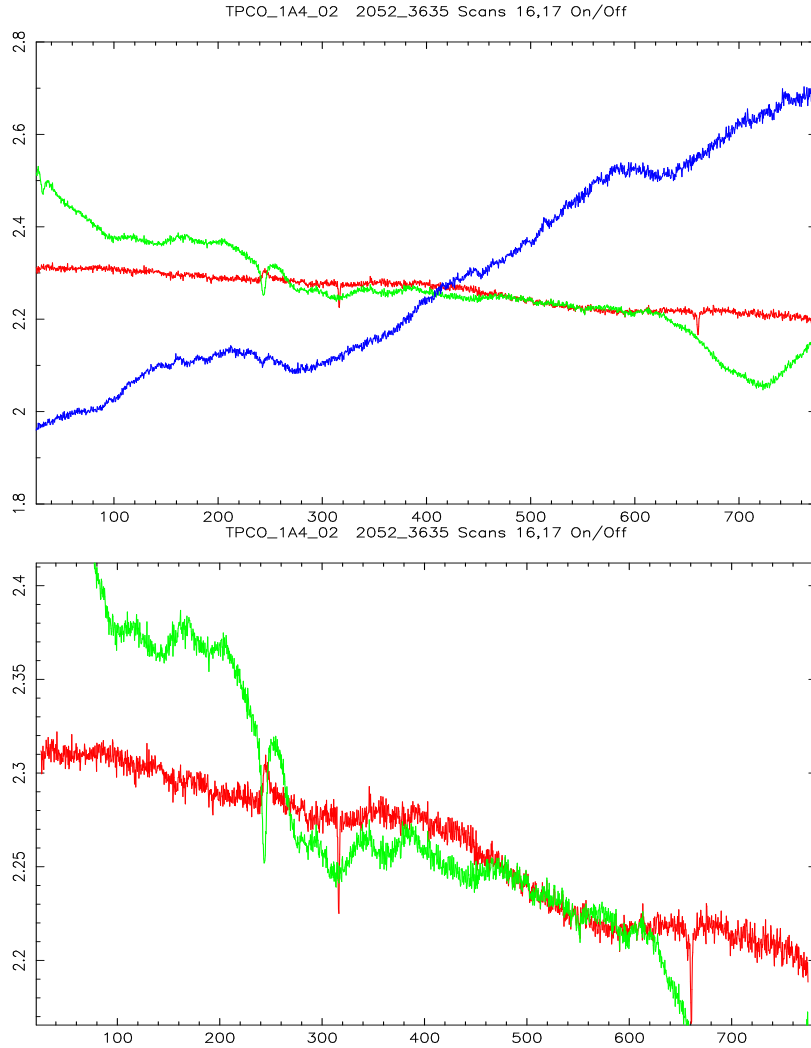


Figure 7: X-band spectral baselines for TPCO1A402 scan pair 16 and 17, on 2052–3635, calculated in three ways. The red trace was calculated using  $T_{rx}$  measured using scan pair 14 and 15, NGC 7027 data, as a Hot/Cold measurement. The green trace was calculated using a constant  $T_{sys}$ , and the blue trace used a  $T_{sys}$  derived from Cal On - Cal Off data in scan 17. The vertical scale corresponds to  $T_{On} - T_{Off}$  in Kelvin. The lower panel shows the red and green traces in more detail. For these plots 400MHz on the horizontal axis corresponds to a sky frequency of 9900MHz, and sky frequency increases to the right. The data was from the RCP polarization.

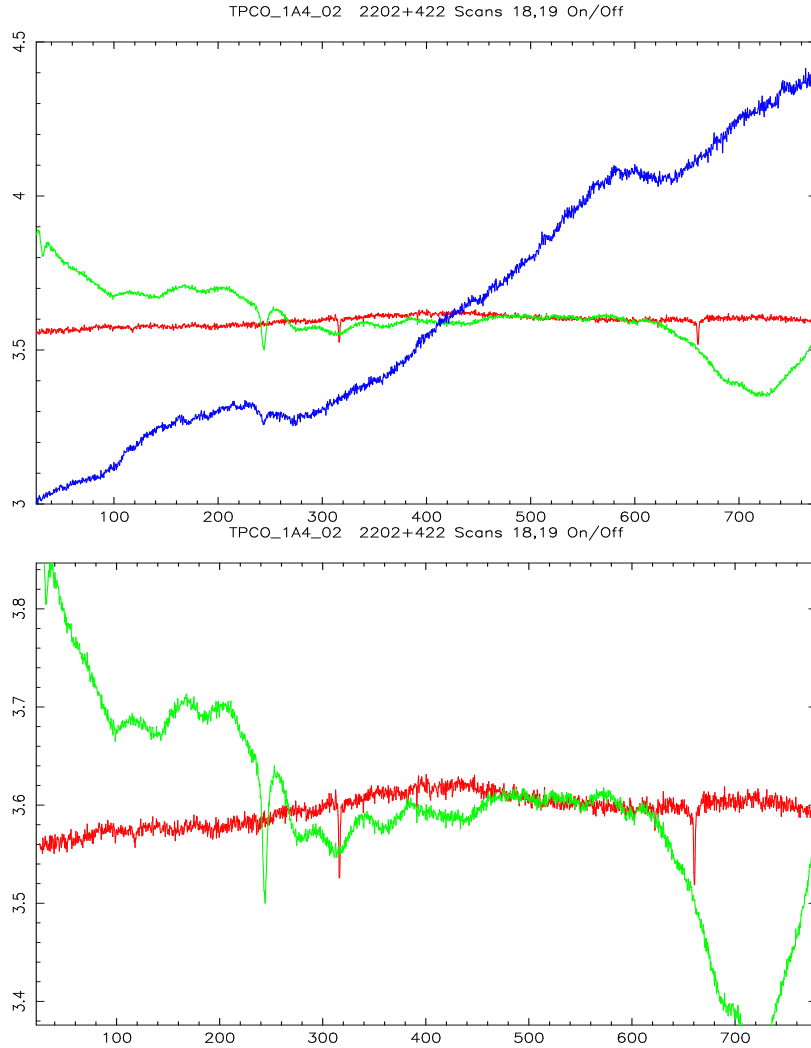


Figure 8: X-band spectral baselines for TPCO1A402 scan pair 18 and 19, on 2202+422, calculated in three ways. The red trace was calculated using  $T_{rx}$  measured using scan pair 14 and 15, NGC 7027 data, as a Hot/Cold measurement. The green trace was calculated using a constant  $T_{sys}$ , and the blue trace used a  $T_{sys}$  derived from Cal On - Cal Off data in scan 19. The vertical scale corresponds to  $T_{On} - T_{Off}$  in Kelvin. The lower panel shows the red and green traces in more detail. For these plots 400MHz on the horizontal axis corresponds to a sky frequency of 9900MHz, and sky frequency increases to the right. The data was from the RCP polarization.

## 6 Conclusions

The understanding of GBT spectral baseline characteristics has significantly improved since the onset of observations. Baseline improvements have been incremental, but significant. The requirements on the GBT hardware are stringent, as in all radio astronomy systems, particularly due to the relatively high intermediate frequencies and broad bandwidths used, and the system complexity caused by the need to support multiple backends and multiple simultaneous spectral observations.

The frequency structure in receiver noise which has a serious impact on continuum source observations requires more research until the causes are well understood. However, in the meantime there is promise in improvements to observing and analysis procedures.

The understanding gained in the course of the baseline investigations could be applied to the design of an “ideal” spectral line receiver. The approach would likely evolve toward a highly integrated design, using quite short transmission lines and a minimum of coaxial interconnections, in an isothermal package. The integration of digital samplers with the microwave front-end should be investigated. It is likely that an improved receiver design would make observations for broad spectral lines much more feasible with the GBT.